Proceedings of 9th International Symposium on Fluid-Structure Interactions, Flow-Sound Interactions, Flow-Induced Vibration & Noise
July 8-11, 2018, Toronto, Ontario, Canada

FIV2018-222

AN EXPERIMENTAL AND NUMERICAL STUDY OF FSI APPLIED TO SAIL YACHT FLEXIBLE HYDROFOIL WITH LARGE DEFORMATIONS

Vanilla TEMTCHING TEMOU
SEAIR, 10 rue chalutier les 2 anges
56100 Lorient France
Ecole Navale, 29240 Brest Armées
vanilla@seair.fr

Odran FAGHERAZZI
ComposiTIC-IRDL
Compositic, 2 Allée copernic
56270 Ploemeur, France
fagheraz@univ-ubs.fr

Benoit AUGIER
IFREMER Brest
1625 Route de Sainte-Anne
29280 Plouzané, France
benoit.augier@ifremer.fr

Jacques André Astolfi
Institut de Recherche de l'Ecole Navale,
Ecole Navale, 29240 Brest Armées
France
astolfi@ecole-navale.fr

David RAISON
SEAir-Foil resource center
10 Rue chalutier les 2 anges
56100 Lorient, France
david@seair.fr

ABSTRACT

The recent use of large aspect ratio and highly loaded composite hydrofoils on sailing boats illustrates the limit of the assumption of rigid body. When flying, the hydrofoil presents large deformations which impact significantly the hydrodynamic loads expected. The present work focuses on an experimental campaign performed on a trapezoidal hydrofoil, made of polyacetate material, in the hydrodynamic tunnel at the Research Institute of French Naval Academy. Large deformations up to 4.5% of the span on the hydrofoil's tip are measured at angle of incidence 10° for Re=0.7×10^6 *calculated at mean chord. Vibration analysis performed on this foil, highlights an increase of its resonance frequencies with bending loading. A coupled approach between the Vortex Lattice Method (VLM) potential flow code, AVL, for inviscid calculations, corrected to consider the viscous component and, an in-house structural code based on beam theory by Finite Element Method (FEM) is developed for this application. The comparisons of simulations show good agreements with experiments in a large range of angles of incidence and flow velocities.*

Key words: *FSI, hydrofoil, AVL, FEM, Beam theory, Xfoil, VLM, panel method.*

NOMENCLATURE

C_L, C_D, C_f: lift, drag and friction coefficients
x, y, z: foil coordinates in chord wise, span wise and orthogonal
V_∞, u_e: upstream, edge velocities
α, AoA: angles of attack
τ_w: shear stress
ρ: fluid density
e: relative Num-Exp displacement discrepancies $\Delta z/y$

1 INTRODUCTION

Hydrofoil technology is used on innovative sailing boats to increase their performances. These underwater appendages generate a lift force which, depending on the case, reduces the heel of the boat by creating a recovery torque or lifts the boat's hull out of the water, decreasing

drag and allowing greater speeds. Hydrofoils are elongated structures, heavily loaded and made of composite materials for lightweight reasons. The use of composites for these lightweight and flexible structures under hydrodynamic loading involves complex FSI due to the strongly anisotropic behavior of the composites. It undergoes large deformations which impact significantly the hydrodynamic behavior of the foil with the appearance of phenomena such as ventilation or cavitation. Foil performances are impacted by theses deformations and must be consider in the design process (Ducoin and Al. [1], Sacher and Al. [2]). The objective of the project is to develop a complete approach, based on a strong coupling between open-source codes URANS OpenFOAM CFD for the fluid analysis and Aster CSD for the structure analysis. The researches go through several steps that lead to CDF/CSD tools dedicated to flexible hydrofoils coupled to experimental measurements for validation.

The study presents an experimental campaign performed on a trapezoidal hydrofoil, made of polyacetate material (POM), in the hydrodynamic tunnel at the Research Institute of French Naval Academy where displacements are measured and vibration analysis is performed. The article will first describe the experimental setup and the vibration analysis. Then, the numerical FSI tool named "FS6R code" will shortly be introduced. Simulations are eventually compared to the measured displacements.

2 EXPERIMENTAL SETUP

2.1 Description

Measurements are carried out in the cavitation tunnel at IRENav on a trapezoidal foil of 0.15m span, 0.1 m base chord and 0.03 m tip chord (aspect ratio of 2.3), displayed in Figure 1. The hydrofoil is mounted horizontally at mid-height in the 192 mm squared test section and the maximum speed flow allowed by the system is 12 m/s. The hydrofoil section is a NACA0015, made of polyacetate material (Young Modulus E=2.9 Gpa and Poisson coefficient ν =0.3) selected to have a flexible structure and significant deformations up to 4% depending on the hydrodynamic loads.
The hydrofoil root section is clamped, the tip section is free and the rotation axis for angle modifications is located at x/C = 0.5 of root section. Experiments are carried out in a range of upstream velocities which corresponds to Reynolds number at mean chord ranging from 0.3×10^6 to 0.7×10^6 and performs for incidences of 2°, 6° and 10°. The structural displacements are measured thanks to a laser telemeter along seven fixed positions on the span and a camera records the distorted foil shape.
Fluid Induced Vibrations analysis is investigated experimentally by a laser vibrometry on the POM foil for different hydrodynamic loads. Implementation of vibration experiments can be founded in [3].

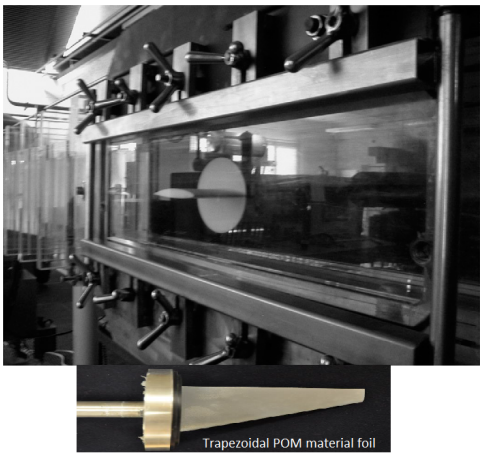

FIGURE 1: *Top: Overview of the hydrodynamic tunnel, bottom: trapezoidal foil in POM material used for experiments.*

2.2 Vibration analysis

Figure 2 shows the velocity vibration spectrum of the structure, investigated at flow speed of $10m/s$ and several incidences. The modal response of the structure is clearly observed with well separated peaks. The first peak corresponds to the first bending mode, the second peak is the second bending mode and the third one is the first twisting mode. For $\alpha = 6°$, the frequencies are founded to be 83.75 Hz, 287.19 Hz and 494.38 Hz respectively.
However, it was observed that the frequency peaks can be shifted (increased or decreased) as a result of the fluid structure coupling that induce non-linearity through inertial (added mass) and stiffness (pre-stress) changes according to the angles of incidence. These results highlight the need to calculate the hydrofoil deformations, induced by the FSI to correctly predict the resonance frequencies. A FSI model is developed to predict such deformations is described in the next part.

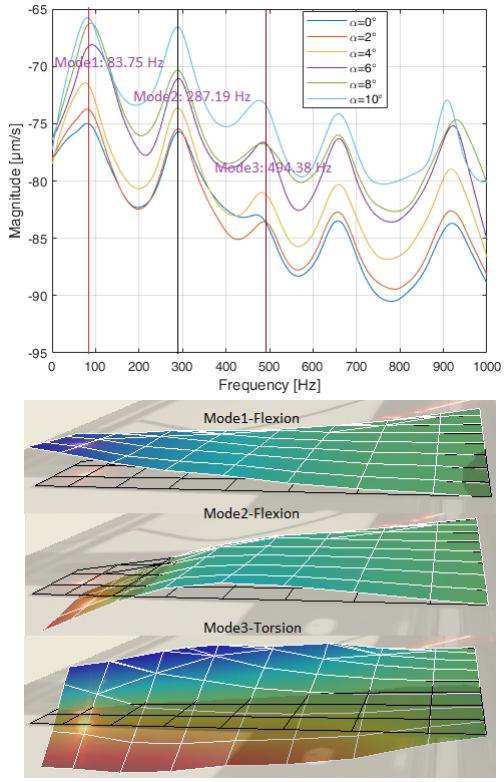

FIGURE 2: *Experimental Velocity vibrations spectrum of the trapezoidal POM foil for u=10 m/s at several incidences and, the modal shapes at 6°.*

3 FS6R

FS6R is a code dedicated to the preliminary stages of foils design to model and to analyze fluid structure interactions. Figure 3 shows the organizational chart of the code, the process is iterative and works from top to bottom as described below.

First, an input file containing the foil geometry, the flow parameters, the structural materials definition and simulation parameters, is defined.

The first block is the geometry and mesh which takes the initial geometry in the input file and prepares the coordinate matrices. Then, the Hydrodynamic block is activated including two main functions: 1.) AVL which performs a VLM inviscid 3D calculations on the whole surface and provides the 3D hydrodynamic coefficients. 2.) XFOIL which performs 2D viscous calculations on each section of the mesh to corrected the initial inviscid assumption. The hydrodynamic coefficients are then transmitted to the structural block. The inputs of the FEM calculation are the initial mesh, the materials definition and the hydrodynamic load distribution. A convergence test block is then applied to the displacement of the structure.

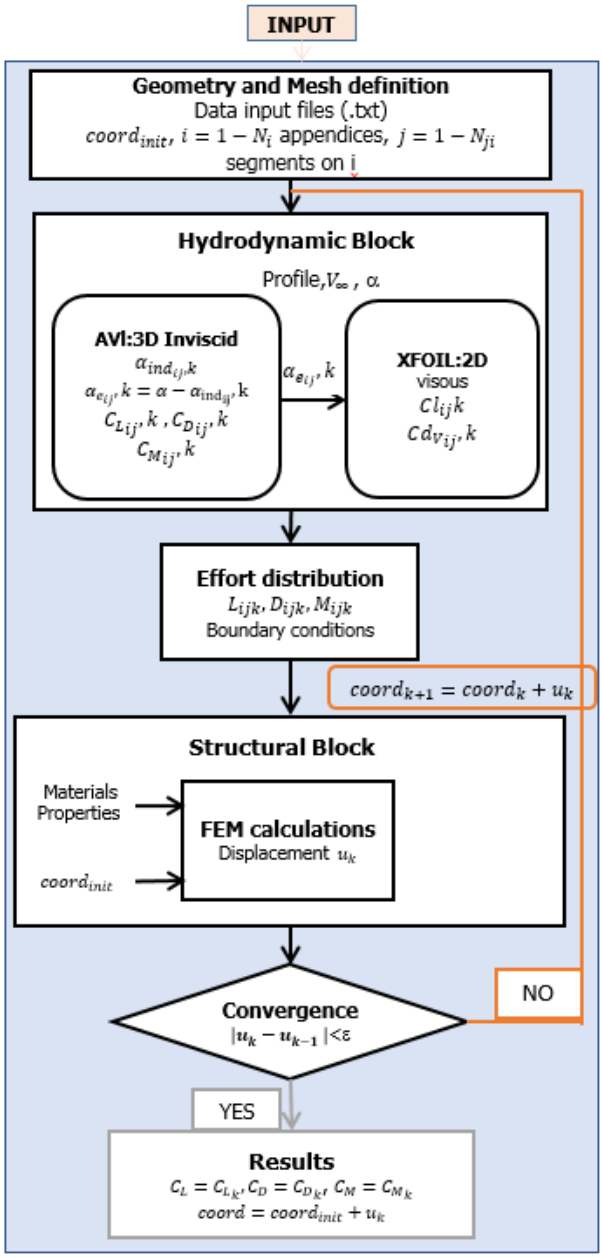

FIGURE 3: *FS6R 's organizational chart describing the iterative loop from the input file to the results.*

The next part describes the hydrodynamic and structural models.

4 DESCRIPTION OF THE NUMERICAL MODEL

4.1 *Vortex Lattice Method and viscous correction*

Athena Vortex Lattice (AVL) is a program based on Vortex Lattice Method [4] to analyze arbitrary configurations of rigid aircraft with lifting surfaces and slender body model. It stands on the potential flow theory and assumes that the lifting surfaces are thin, and modeled with horseshoe vortices distributed along the span and chord while neglecting the influence of viscosity and thickness. Figure 4 shows the foil discretization into 3N panels in both spanwise and chordwise. Lifting line on each panel is a vortex line normal to the section, located at $1/4$ of the panel width in chordwise and to satisfy Thompson law at root and tip, the vortex is aligned with incident flow and extended to infinity. The calculation point in a panel is located at $3/4$ in chordwise and $1/2$ in spanwise.

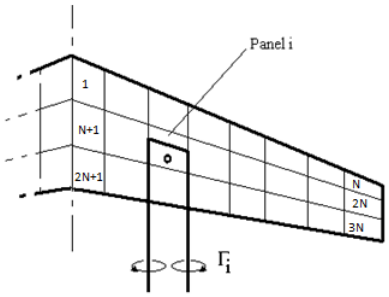

FIGURE 4: *Structure meshing for AVL analysis.*

In agreement with Biot Savart law, a vortex intensity Γ creates an induced velocity w normal to initial flow velocity (equation 1). Regarding the geometry with some transformations, vortices on each panel can be calculated by solving the system in equation 2.
dl is a length element on lifting line, r, the radius between dl and the calculation point, $[A_M]$, the influence matrix consisting of geometrical terms, $[\Gamma]$, the vector of vortex on each panel and $[b_N]$, the boundary conditions.
This induced velocity modifies the effective angle of attack α_e (equation 3), creating an induced angle of attack α_i, which impacts lift coefficient (equation 4). α_o is the zero lift angle and y, the position along the span.
Lift force per panel is calculated with Kutta- Joukowsky theorem. Equations 5 and 6 show the total induced drag and the total lift forces calculated as the sum of each panel contribution. AVL takes as input a geometry file containing the surfaces defining the structure, the meshing parameters and a run file describing the configurations to simulate. A surface is defined by sections and a section consists of x, y, and z coordinates of the profile's leading edge and the profile's type.

$$w = \frac{\Gamma}{4\pi}\frac{dl \times r}{r^3} \tag{1}$$

$$[A_M] \times [\Gamma] = [b_N] \tag{2}$$

$$\alpha_i = tan^{-1}\left(\frac{w}{V_\infty}\right), \alpha_e = \alpha - \alpha_i \tag{3}$$

$$C_L(y) = C_l\left[\alpha_e(y) - \alpha_o(y)\right] \tag{4}$$

$$L = \rho V_\infty \int_{-b\frac{w}{2}}^{b\frac{w}{2}} \Gamma(y)dy \tag{5}$$

$$D_i = -\frac{\rho}{2}\int_{-b\frac{w}{2}}^{b\frac{w}{2}} \Gamma(y)w(y)dy \tag{6}$$

The AVL invscid approach is corrected using Xfoil [5]. It incorporates a two-equation integral formulation of the viscous boundary layer and the approximate e_N envelope method [6]. It allows the prediction of transition points and separation bubble, through the resolution of the boundary layer and the transition equations which is based on a Newton method. It is compared with other CFD methods and solvers in [7]. Overall, XFOIL is simple to use and has a reasonable computation cost on a classical workstation, in most of the cases, making it a natural candidate to be coupled with a structural solver (see XFOIL implemented in [8], for FSI on wind blade or [4], for FSI on hydrofoils).

4.2 Beam theory by finite elements

The hydrofoil is modeled by a 3D Euler-Bernoulli beam with a linear static structural behavior. This beam is prismatic and made of a single isotropic and homogeneous material. The beam is characterized by its neutral axis (along x) and a straight cross-section within the (y, z) plane. The section stays straight even after deformation and, is studied using its principal inertial coordinate system. This kind of beam has the following displacement field: $\vec{u}(x,y,z) = \vec{\tilde{u}}(x) + \vec{\tilde{\theta}}(x) \wedge (y\vec{e_y} + z\vec{e_z})$.
$(\vec{\tilde{\theta}}, \vec{\tilde{u}})$ is the displacement screw with a moment $\vec{\tilde{u}} = (\tilde{u}_x, \tilde{u}_y, \tilde{u}_z)$. This moment matches the neutral axis displacements, its resultant $\vec{\tilde{\theta}} = (\tilde{\theta}_x, \tilde{\theta}_y, \tilde{\theta}_z)$ matches the cross-section rotations.

Besides the linkage reactions loads, the beam is subjected to distributed forces $\vec{q}$ and a torsional torque M_x. The beam's internal loads are depicted by an internal tensor $\{\tau\}$. With the torsion allowed, the strain and stress tensors have only three components different from zero: xx, xy and xz. The beam constitutive laws are described by the Euler Bernoulli theory.

The problem is solved using the displacement Finite Element Method. Many open source tools are available such as Aster, FEnics Project, Calculix or CALFEM [9] and CALFEM Matlab toolbox has been chosen as a starting base in our structural development. Its integration beside the fluid simulation part is simple and moreover, CALFEM is easily customizable for future composite foil simulations.

One can prove [9] that the problem solution $(\vec{\theta},\vec{u})$ matches the displacement field by minimizing the elastic potential energy E_p. E_p is a function of the strain energy and the work of the external loads depicted in equation 7. The beam is discretized within N elements, with two nodes each. A node i, is characterized by six degrees of freedom, six nodal loads and six shape functions (one per degree of freedom). The shape functions are chosen linear, and cubic by using Euler-Bernoulli relations. For an element e, the strain energy and the work of external loads are given by equations 8 and 9.

$\{U^e\}$is the nodal displacement vector and $[Ke]$ the element stiffness matrix. $[Ke]$ is expressed using the cross-section properties as explained in [10]. $\left\{f^e_{nod}\right\}$ stands for the loads which are directly applied to the nodes. $[Ke]$ and $\left\{f^e_d\right\}$ are assembled using the method described in [9] to obtain the global linear system in equation 10, that we need to solve with boundary conditions.

$$E_p = E_{def} - W_{ext} \tag{7}$$

$$E_{def} = \frac{1}{2}\{U^e\}^T [K_e]\{U^e\} \tag{8}$$

$$W_{ext} = \{U^e\}^T (\{f^e_d\}) + \{f^e_{nod}\}) \tag{9}$$

$$F = [K]U \tag{10}$$

4.3 Comparison between FSI and rigid simulation

The large deformations due to FSI on the foil are expected to change the hydrodynamic loads. Figure 5 presents the lift, drag and pitching moment coefficients along the span computed with FS6R on the trapezoidal POM foil at 10° compared with rigid foil computations for several Reynolds numbers. For all the configurations, it is observed that the rigid foil's hydrodynamic coefficients are significantly different from the FSI curves, highlithing a general hydrodynamic behavior for the deformed foil. In this case, the deformed foil has a better Cl/Cd, mainly due to a strong decrease of drag. These hydrodynamic coefficients will be experimentally investigated in an upcoming test campaign.

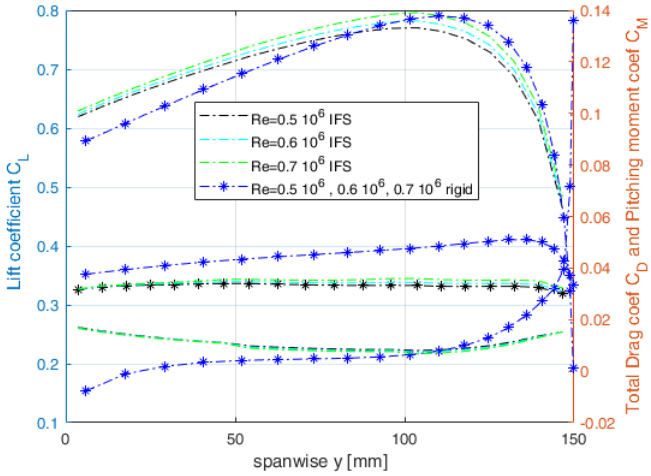

FIGURE 5: *Lift, drag and pitching moment coefficients along the span for trapezoidal POM foil, $\alpha = 10°$ for flexible and rigid foil at different Re*

4.4 Numerical and experimental Comparisons

Comparisons are focused on the deformations of the foil. During experiments, the load were not recorded due to the clamping system used to support the POM foil.

Figure 6 compares experimental and numerical results for $\alpha = 10°$ at various upstream velocities. The vertical axis corresponds to the vertical displacement of the foil and the horizontal axis is the span. The structure moves vertically as a consequence of the lift effect. Numerical and experimental results match very well along the span. However, discrepancies are observed near the tip.

Figure 6 shows that the simulation slightly over estimate the displacement in the considered cases. The main reason could be that the viscous correction is only added to the drag force when the lift is based on the inviscid

approach. To assess the difference between the two approaches, the coefficient e is calculated for each measure as $e(y) = \frac{(\Delta Z_{num}(y) - \Delta Z_{expe}(y))}{y}$.
For the whole experiments investigated, e is less than 0.7%, indicating that FS6R is in good agreement with experiments.

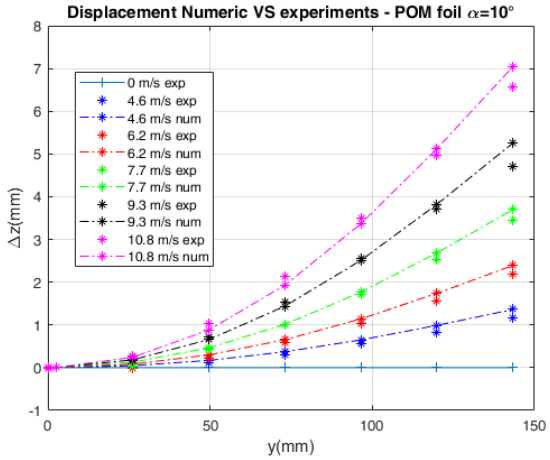

FIGURE 6: *Foil's displacements for various velocities at* $\alpha = 10°$.

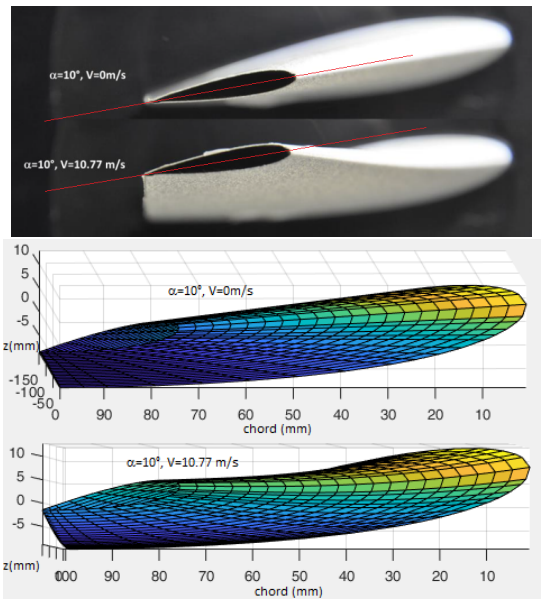

FIGURE 7: *Experimental tip displacement and numerical shape of the foil for* $\alpha = 10°$ *at velocity 10.77 m/s.*

Figure 7 shows the experimental shape recorded with the camera and the calculated numerical shape of the distorted foil at 10.77 m/s and 10° of incidence. As shown, they are very similar. However, no twist has been recorded experimentally while numerically there is an existing twist of 0.9° at the tip for this configuration. This existing twist is in agreement with the numerical overestimation of the tip displacement. This difference can come on one hand, from the limitation of the VLM and beam theories appearing for structures with aspect ratio lower than 4-5 and moreover, confinement effects in the tunnel might be considered as well. On the other hand, inviscid fluid assumptions for the lift computation can lead to this over prediction.
Figure 8 gives the evolution of the tip displacement as a function of the upstream velocity for incidences of 2°, 6° and 10°. Numerical and experimental results match with a good accuracy.

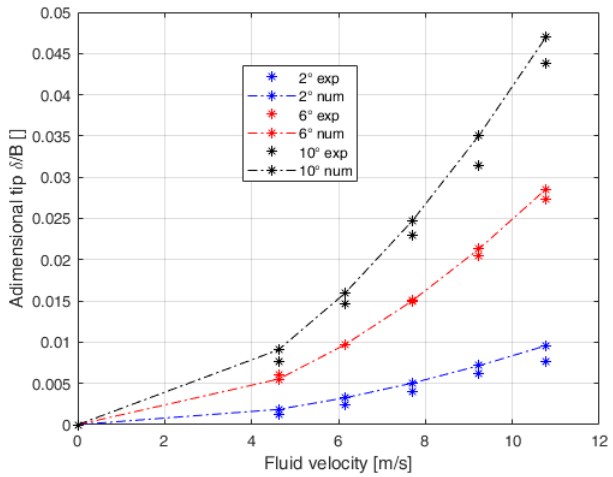

FIGURE 8: *Foil's tip vertical displacement versus upstream velocity for different angles of incidence.*

5 CONCLUSION

This paper presents an experimental and numerical comparison based on experiments performed on a flexible hydrofoil in POM materials. The hydrofoil is tested in an hydrodynamic tunnel at different speeds and incidences. The deformations observed are large up to 4% and have a significant impact on the foil 's hydrodynamic performances. Vibrations analysis of the foil show a fluid struc-

ture coupling which induces non-linearity through inertial (added mass) and stiffness (pre-stress) changes according to the angles of incidence. A numerical approach of fluid structure coupling "FS6R", based on VLM and FEM method is developed to simulate these large deformations. Numerical and experimental comparison based on displacement give very good results. Future developments on FS6R will be dedicated to the consideration of composite structures, free surface for ventilation phenomenon and cavitation.

ACKNOWLEDGEMENTS

The authors wish to acknowledge the technical and administrative staff of the French Naval Research Academy for their support during all hydrodynamic tests.

References

[1] A. Ducoin, F. deniset, J. A. Astolfi 2009. "Numerical and Experimental Investigation of Hydrodynamic Characteristics of Deformable Hydrofoils". *Journal of Ship Research, Vol. 53, No. 4, December 2009, pp. 214226*

[2] Matthieu Sacher, M. Durand, E. Berrini, F. Hauville and R. Duvigneau and O. Le Maitre, J. A. Astolfi, 2018. "Flexible hydrofoil optimization for the 35th America's Cup with constrained EGO method". *"Ocean Engineering", Vol. 157, No. 0029-8018, pp. 62 - 72*

[3] A. Lelong, J. A. Astolfi,P. Guiffant, 2017 . "An Experimental Analysis of the Structural Response of Flexible Lightweight Hydrofoils in Cavitating Flow". *Journal of Fluids Engineering. 140. 10.1115/1.4037990.*

[4] Kinga Budziak, Prof. Dr.-Ing. Dieter Scholz, MSME, 2015. "Aerodynamic Analysis with Athena Vortex Lattice (AVL)". *Master Project, Department of Automotive andAeronautical Engineering Hamburg University of Applied sciences.*

[5] Drela, M., 1989 "XFOIL: an Analysis and Design System for Low Reynolds Number Airfoils". *Springer Berlin Heidelberg, Berlin, Heidelberg, ISBN 978-3-642-84010-4, pp. 112. https://doi.org/10.1007/978-3-642-84010-4-1.*

[6] Van Ingen, J., 2008. "The eN method for transition prediction: historical review of work at TU Delft". *38th Fluid Dynamics Conference and Exhibit. American Institute of Aeronautics and Astronautics, Seattle, United States, pp. 149*

[7] Morgado, J., Vizinho, R., Silvestre, M., Pascoa, J., 2016. "XFOIL vs CFD performance predictions for high lift low Reynolds number airfoils". *3Aerosp. Sci. Technol. ISSN: 1270-9638 52, 207214. https://doi.org/10.1016/j.ast.2016.02.031. http://www. sciencedirect.com/science/article/pii/S1270963816300839.*

[8] MacPhee, D., Beyene, A., 2013. "Fluid-structure interaction of a morphing symmetrical wind turbine blade subjected to variable load". *Int. J. Energy Res. ISSN: 1099-114X 37 (1), 6979. https://doi.org/10.1002/er.1925.*

[9] P-E. Austrell, 1992 - 2004,"CALFEM manual, a finite element toolbox version 3.4 ". *Copyright 1992 2004 by the Division of Structural Mechanics at Lund University. All rights reserved*

[10] O.C. Zienkiewicz, 2013 "The Finite Element Method: Its Basis and Fundamentals, In The Finite Element Method: its Basis and Fundamentals" . *(Seventh Edition), Butterworth-Heinemann.*